






A Comparative Study of Bond Test Methods for Externally Bonded FRCM and SRG Composites

Marco Frallonardo¹, Lesley H. Sneed²(✉) , Tommaso D'Antino³ ,
and Christian Carloni⁴ 

¹ Department of Civil, Chemical, Environmental, and Materials Engineering,
University of Bologna, Viale Risorgimento 2, 40136 Bologna, Italy

² Department of Civil, Materials, and Environmental Engineering, University of Illinois at
Chicago, 929 W Taylor St, Chicago, IL 60607, USA
lhsneed@uic.edu

³ Department of Architecture, Built Environment, and Construction Engineering, Politecnico di
Milano, Via Ponzio 31, 20133 Milan, Italy

⁴ Department of Civil Engineering, Case Western Reserve University, 10900 Euclid Ave,
Cleveland, OH 44106, USA

Abstract. The bond behavior of externally-bonded fiber reinforced composites has been studied experimentally using different types of test methods. In this study the bond behavior of composite strips externally bonded to fired-clay brick masonry was tested using single-lap direct shear tests and hinged beam tests. The results obtained from the two test types were compared to investigate the effect of the test set-up on the load-carrying capacity of the matrix-fiber interface. Two different composite systems were considered: a fiber-reinforced cementitious matrix (FRCM) composite with a balanced bidirectional mesh of basalt fibers embedded in a hydraulic lime-based mortar, and a steel reinforced grout (SRG) with a sheet of ultra-high-strength unidirectional steel fiber cords embedded in the same mortar. The results are discussed and compared in terms of failure modes and applied load versus slip of the fibers response. An estimate of the matrix-fiber interfacial fracture energy of SRG-masonry joints is proposed using a global energy balance approach that does not require measurement of the strain in the fibers.

Keywords: Bond · Fiber-Reinforced Cementitious Matrix (FRCM) composite · Hinged Beam Test · Single-Lap Shear Test · Steel-Reinforced Grout (SRG) composite

1 Introduction

Natural hazards, such as earthquakes, have proved the inadequacy of certain masonry arch structures to withstand lateral loads. Strengthening solutions are required to increase the service life of existing structures and prevent certain collapse mechanisms of the

structure. In the case of masonry arches, the crack pattern is characterized by localized damage producing structural hinges. A collapse mechanism is characterized by the development of a number of structural hinges equal to or larger than four [1–5].

The collapse mechanism of an arch can be modified by adding reinforcement to the extrados, to the intrados, or to both surfaces such that the formation of hinges is delayed [4, 6]. Different types of reinforcement have been explored for strengthening of masonry structures, especially fiber-reinforced polymer (FRP) composites since they can be bonded in situ to the surface of an existing structure. However, an important failure mode of this type of strengthening system is debonding of the composite, resulting in loss of composite action. The debonding mechanism of FRP systems bonded to a masonry substrate has been investigated in several experimental campaigns [7, 8]. However, due to the polymeric matrix, FRP composites exhibit poor behavior at high temperatures and lack of reversibility of the application. In addition, FRP composites have a low vapor compatibility with masonry substrates.

To overcome some of the disadvantages of traditional FRP systems, a new family of composites, known as fiber- or fabric-reinforced cementitious matrix (FRCM) composites, was recently developed. FRCM composites consist of continuous fibers embedded within an inorganic matrix that is responsible for the stress transfer between the composite and the substrate and between the matrix and fibers. FRCM composites offer several advantages when compared to traditional FRP composites: 1) the cementitious material poses less of a toxicity concern compared to the epoxy resins required in FRP systems; 2) the cementitious material provides better performance under high heat conditions; 3) the cementitious material provides better resistance to UV radiation; and 4) the cementitious material is not adversely affected by the presence of excess water. FRCM composites also exhibit partial reversibility.

FRCM composites have proven effective in strengthening of historical masonry structures [4, 9–11]. Steel-FRCM, also referred to as steel reinforced grout (SRG) composite, which consists of high-strength steel fibers embedded in a cementitious or lime-based grout, have gained interest in masonry strengthening applications [9, 10, 12]. Basalt-FRCM has also been used to strengthen masonry arches, highlighting the good mechanical properties of basalt fibers and their low cost [6, 13].

Different test methods have been used to study the bond behavior of FRCM-masonry joints, including single- and double-lap direct shear tests, as well as beam tests [14, 15]. Direct shear tests are easier to construct and to test, whereas beam tests may be more representative of strengthened structural members. Additional background on the study of bond behavior, and the influence of factors such as surface preparation and matrix curing conditions, is provided in ACI 549.6R [16]. In this study, the bond behavior of SRG-masonry joints and basalt FRCM-masonry joints was studied using two different tests: the direct single-lap shear test and a hinged beam test. The hinged beam test was designed to simulate the opening of a structural hinge in an arch. Load responses are presented, and failure modes are discussed. A comparison of the results obtained by the two tests is presented.

2 Materials

This study investigated the behavior of low-density SRG and low-density basalt-FRCM composite systems bonded to masonry block substrate. The Rosso Vivo bricks used to construct the masonry blocks were supplied by the company San Marco – Terreal Italia. The compressive strength of the bricks, determined from the average of 10 specimens tested in accordance with UNI EN 772-1 [17], was 20.8 MPa [coefficient of variation (CoV) = 0.184].

The masonry blocks were bound together using a natural plaster made with pure lime NHL (natural hydraulic lime) according to EN 459-1 [18]. The mortar mixture used to construct the specimens was intended to represent the mechanical behavior of weak mortars, thus reproducing existing historical structures. The compressive strength was determined experimentally for each batch of mortar used to construct the masonry blocks. The average compressive strength, determined by 50.8 mm cubes in accordance with ASTM C109/C109M [19], was 2.9 MPa (CoV = 0.024).

The matrix used for both the SRG and basalt-FRCM composites was made of lime NHL, suitable for both composites. It is a classified M15 mortar, according to EN 998-2 [20], and contains only natural raw materials and recycled minerals [21]. The splitting strength of each mortar matrix was determined from three 50.8 mm diameter \times 101.6 mm long cylinders sampled from each batch and tested at 28 days in accordance with ASTM C496 [22]. The average splitting tensile strength of all mortar batches was 1.13 MPa (CoV = 0.062).

The steel fibers used in the SRG composite were in the form of a unidirectional sheet made of ultra-high-strength galvanized steel micro-cords, fixed to a fiberglass micromesh that facilitates sheet installation. The sheet density was 1.57 cords/cm, and the area density was approximately 670 g/m². According to the manufacturer [21], the fiber sheet had a tensile strength of >3000 MPa, and the Young's modulus was >190 GPa.

The basalt fibers used in the basalt-FRCM composite were in the form of a balanced bidirectional mesh with an alkali-resistant protective treatment made of solvent-free, water-based resin and stainless steel micro-filaments welded together. The equivalent thickness of the mesh was 0.032 mm, and the area density was approximately 200 g/m². According to the manufacturer [21], the tensile strength was >1700 MPa, and the Young's modulus was >70 GPa.

3 Experiments

3.1 Test Specimens

A total of 17 specimens were tested in this study. Nine specimens were used for the single-lap direct shear tests, and eight specimens were used for the beam tests. All specimens included a composite strip with a single layer of fibers. The main test variable was FRCM fiber type, however the composite bonded length also varied slightly between the two test types.

In the single-lap shear tests, all specimens had a composite bonded length of 270 mm and a composite bonded width of 50 mm for consistency with specimens reported in

literature [12]. The bonded width of 50 mm corresponded to eight fiber cords for SRG and three fiber bundles for basalt-FRCM. The thickness of the composite matrix was 5 mm (total) and was controlled by formwork applied to the masonry block during application.

Regarding the beam tests, the composite bonded length on each of the two blocks was 250 mm, and the composite bonded width was 50 mm for all specimens. Similar to the single-lap shear tests, a bonded width of 50 mm corresponded to eight fiber cords for SRG and three bundles for basalt-FRCM. The matrix thickness was 5 mm (total).

The specimens were named following the notation TEST-X-Y-A-RN-Z, where TEST indicates the type of test (DS = single-lap direct shear test, BT = beam test), X = bonded length (ℓ) in mm, Y = bonded width (B_f) in mm, A indicates the type of fiber (S = low-density steel, LDB = low-density basalt), RN represent the load rate (N = times the standard rate R, which is equal to 0.00084 mm/s), and Z = specimen number.

3.2 Single-Lap Shear Tests

The single-lap shear test specimen was comprised of a masonry prism (block) to which a strip of composite was bonded to one surface. Figure 1 shows a photo of the single-lap shear test. A steel plate was affixed to the base of the machine. The specimen was constrained by a steel frame fastened to the plate with four bolts. Since the substrate block height was slightly variable, thin plates were placed between the restraint frame and the top of the block, creating a uniform surface that helped to provide a uniform pressure during the test. Two steel plates were fastened and glued to the loaded end of the fiber strip which was left bare outside the composite bonded region; the steel plates were gripped by the testing machine. Two-component epoxy resin was used to bond the plates to the fiber strip to avoid slippage between the fibers and steel plates that could lead to anomalies of the results.

The applied load and machine stroke were measured with the servo-hydraulic universal testing machine. In addition, two DC-LVDTs (direct-current linear variable differential transformers) with a measurable range of ± 25 mm were mounted to the surface of the specimen to measure the slip of the fibers at the loaded end of the composite relative to the substrate. The load rate of the testing machine was controlled by the average of readings of two DC-LVDTs. A steel “omega” shaped plate was bonded to the fiber strip outside the composite bonded region to provide a reaction for two DC-LVDTs (see Fig. 1b). Regarding the SRG composite, the steel omega was bonded to the first transversal fiberglass bundle outside the composite bonded region. This location was selected to reduce the influence of the elastic elongation of the steel fibers on the measured global slip values. Conversely, in order to obtain the ideal failure of basalt-FRCM composite, frequently reported to be located immediately outside the composite bonded region, the steel omega plate was bonded to the third transverse bundle outside the bonded region.

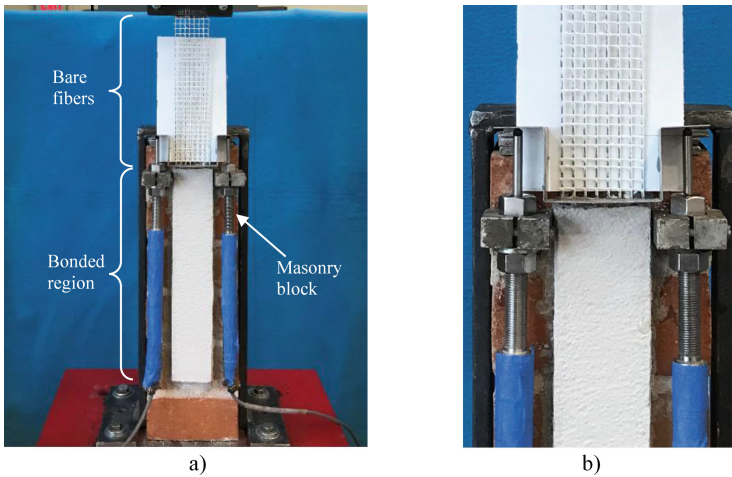


Fig. 1. Single-lap shear test: a) photo of SRG-masonry joint specimen, b) close up view of LVDTs at loaded end of the SRG composite and bare fibers outside the bonded region.

3.3 Hinged Beam Tests

The hinged beam test specimen was comprised of two masonry prisms (blocks) aligned end to end with a small gap in between them and a strip of composite bonded to both prisms (see Fig. 2a). Figure 2b shows a photo of the hinged beam test. The specimen was placed on top of a steel base mounted on the base of the testing machine and supported by two steel rollers at the ends of the blocks. An aluminum cylinder between the two blocks behaved like a hinge. It should be noted that the support rollers were free to translate such that the lateral displacement of the two blocks permitted the opening of the hinge (i.e., the specimen was restrained only by the composite).

The loading fixture consisted of two aluminum cylinders and an aluminum plate placed on two grooved aluminum plates on top of the specimen (one on each block). The two cylinders were aligned with the beginning of the bonded area of the two composite strips. Finally, a steel ball was placed in the center of the loading plate between the loading fixture, and a loading plate was attached to the universal testing machine to distribute the load.

The load was applied by controlling the machine stroke until failure of the specimen. The loading rate of the R1 specimens was fixed at 0.00252 mm/sec such that the composite strip was effectively loaded at approximately the same rate used for the single-lap shear test. During the test, the applied load and machine stroke were measured with the load cell of the universal testing machine. In addition, four DC-LVDTs were used, two of which measured the vertical displacement of the specimen under the loading points, and the other two measured the vertical displacements of the supports.

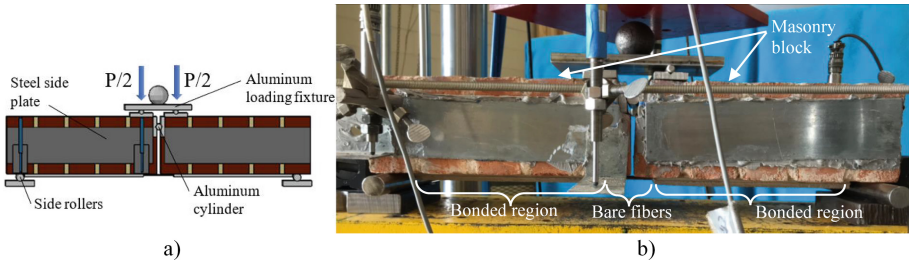


Fig. 2. Hinged beam test: a) schematic, b) photo of test setup.

4 Discussion of Results

4.1 Single-Lap Shear Tests

Table 1 summarizes the single-lap shear test results in terms of failure mode, peak load, peak (axial) stress in the fiber (determined as the peak load divided by the cross-sectional area of the longitudinal fibers), and the loaded end (global) slip (computed as the average of the LVDT readings) at the peak load for each specimen. Figure 3a and 3b show the load responses of the SRG-masonry joints and the basalt-FRCM-masonry joints, respectively.

Regarding the specimens with SRG composite, two different failure modes were observed: detachment of the SRG strip from the substrate (SD) and interlaminar failure at the matrix-fiber interface (MF). The shape of the load response of SRG-masonry joints was affected by the failure mode, as shown in Fig. 3a, where the grey curves are associated with SD failure and the blue curves with MF failure.

The basalt-FRCM joints failed due to rupture of the basalt fibers (FR). If the fiber bundles ruptured simultaneously (only for specimen DS_270_50_LDB_R1_3), the load response was a relatively smooth, always ascending curve, as shown in Fig. 3b. If one bundle failed first, the load response exhibited drops, each one corresponding to rupture of a single bundle. It should be noted that the loading branch after the load drop occurred had a lower stiffness due in part to the reduction of the area of the fibers.

4.2 Hinged Beam Tests

Table 2 summarizes the hinged beam test results in terms of failure mode, peak applied load, and deflection at peak load for each specimen. Figure 4a and 4b show the applied load versus deflection curves for all the beam specimens reinforced with SRG and basalt-FRCM strips, respectively. The deflection was determined by averaging the two LVDT measurements at midspan and subtracting the average of the two LDVDT displacement readings at the supports.

In order to examine the response of the composite, values of the applied load and deflection of the hinged beam were used to determine the applied load and global slip of the fibers at the start of the composite bonded region. The applied force in the fibers F_f can be computed by considering the equilibrium of the free body diagram of Fig. 5a:

$$F_f = \frac{1}{L_1} \left(\frac{PL_2}{2} + \frac{qx_1^2}{2} - \frac{x_2^2}{2} \right) \quad (1)$$

Table 1. Direct shear test results.

Specimen ID	Composite	Failure mode	Peak load [kN]	Peak stress [MPa]	Global slip at peak load [mm]
DT_270_50_S_R1_1	SRG	SD	7.49	1784	1.29
DT_270_50_S_R1_2	SRG	SD	10.45	2489	2.75
DT_270_50_S_R1_3	SRG	SD	10.16	2419	1.91
DT_270_50_S_R1_4	SRG	MF	6.74	1604	0.84
DT_270_50_S_R1_5	SRG	MF	11.39	2711	2.51
DT_270_50_S_R1_6	SRG	MF	5.87	1398	1.62
DT_270_50_LDB_R1_1	Basalt-FRCM	FR	1.35	841	1.01
DT_270_50_LDB_R1_2	Basalt-FRCM	FR	1.42	888	1.50
DT_270_50_LDB_R1_3	Basalt-FRCM	FR	1.59	991	1.46

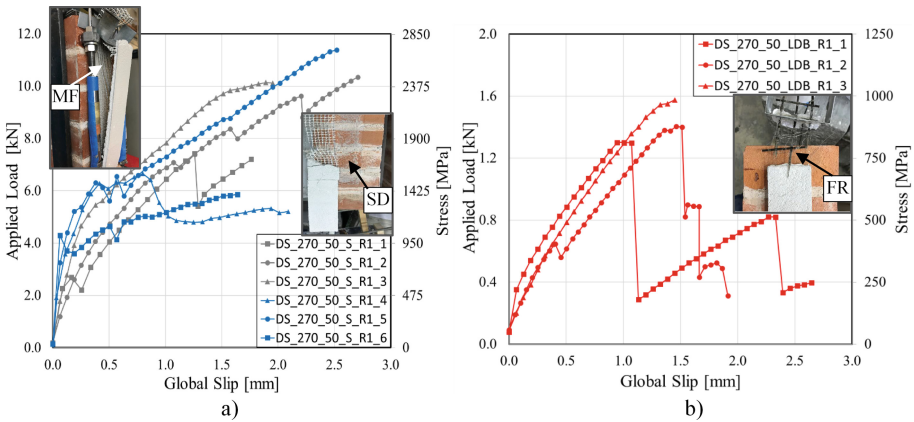


Fig. 3. Applied load-global slip response for direct shear test specimens with a) SRG (grey curves: failure mode SD; blue curves: failure mode MF) and b) basalt-FRCM (red curves: failure mode FR).

where L_1 and L_2 are the vertical and horizontal arms, respectively. The self weight q was considered as uniformly distributed along the length of the block ($x_1 + x_2$). The weight of each block was measured after the test. The contribution of the self weight was very small compared to the load P to which the specimen was subjected.

The rotation of the masonry blocks during the test resulted in a vertical displacement of the aluminum cylinder between the two blocks, which was horizontally and vertically restrained by the blocks and behaved as an internal hinge. This vertical displacement was proportional to the deflection measured at midspan, which was used to determine the angle θ that defines the rotation of the blocks. The slip of the fibers was computed by enforcing compatibility. The opening of the blocks at the level of the fibers must be

Table 2. Hinged beam test results.

Specimen ID	Composite	Failure mode	Peak load [kN]	Deflection at peak load [mm]	Peak force applied in the fiber [kN]	Peak stress [MPa]	Global slip at peak load [mm]
BT_250_50_S_R3_1	SRG	MF	7.71	3.54	9.64	2295	0.99
BT_250_50_S_R3_2	SRG	MF	6.50	3.47	8.14	1939	1.03
BT_250_50_S_R3_3	SRG	MF	7.22	5.45	9.35	2227	1.77
BT_250_50_LDB_R1_1	Basalt-FRCM	FR	0.89	2.31	1.20	752	0.61
BT_250_50_LDB_R3_2	Basalt-FRCM	FR	1.02	2.67	1.36	852	0.71
BT_250_50_LDB_R3_3	Basalt-FRCM	FR	0.88	2.05	1.19	744	0.51
BT_250_50_LDB_R3_4	Basalt-FRCM	FR	1.20	2.67	1.58	989	0.66

equal to the slip of the fibers at the beginning of the two bonded areas plus the elastic elongation of the fibers in between the two bonded areas. The slip was assumed to have the same magnitude at the beginning of the two bonded areas, i.e., the global slip of the fibers was the same for both blocks.

Considering Fig. 5b, it can be shown that $L_2\theta = s$, and $L_1\theta = s'$, where s is the deflection measured from the difference between the average of the midspan LVDT readings and the average of the support LVDT readings, while s' is the opening of the two blocks measured at the level of fibers. It should be noted that given the magnitude of the angle θ , the following approximations were made: $\cos\theta \approx 1$ and $\sin\theta \approx \theta$.

The relationship between the elongation of the fibers, the global slip g , and the rigid horizontal displacement s' is:

$$\frac{F_f}{E_f b_f t_f} \left(\frac{L_{free}}{2} \right) + g = s' \quad (2)$$

where L_{free} is the distance between the two bonded areas, and E_f , b_f , and t_f are the Young's modulus, width, and thickness of the fibers, respectively.

Using the procedure above, the entire load response was computed for each composite strip. Table 2 summarizes the applied force and stress in the fibers, and the global slip at peak load for the SRG-masonry joints and basalt-FRCM-masonry joints. Figure 4c and 4d show the applied force in the fibers versus the global slip for all beam specimens reinforced with SRG and basalt-FRCM, respectively.

4.3 Comparison of Single-Lap Direct Shear Tests vs. Beam Tests

This section compares the results of the single-lap direct shear and hinged beam tests to determine if the different test types produced similar results. Specimens that failed due to detachment from the substrate (SD) were neglected from the comparison. In

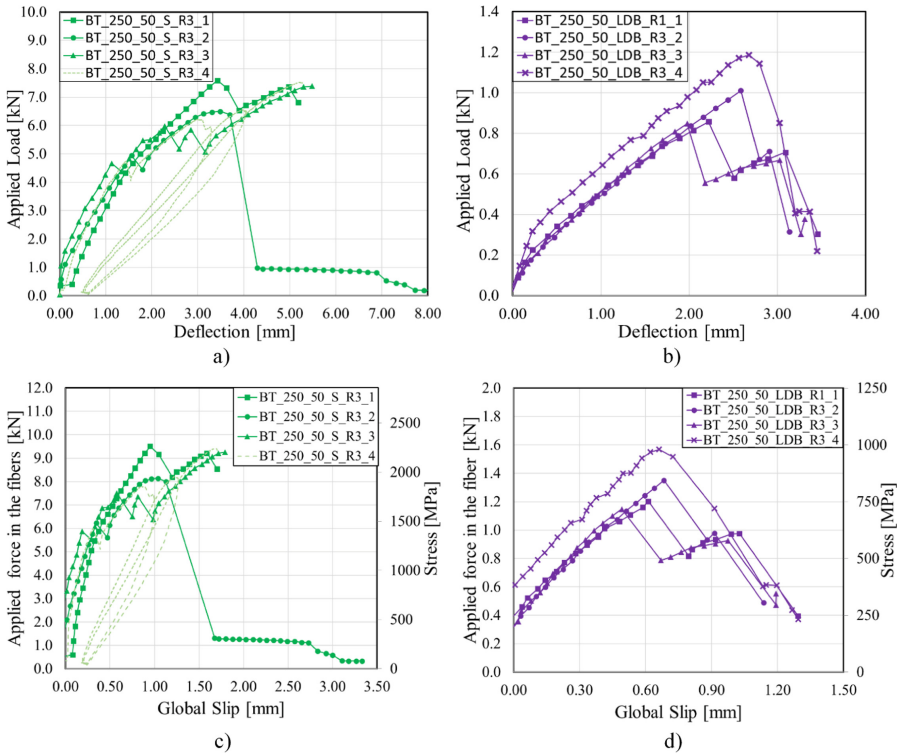


Fig. 4. Hinged beam tests: a) load-deflection response for specimens with SRG; b) load-deflection response for specimens with basalt-FRCM; c) load-global slip response for specimens reinforced with SRG; d) load-global slip response for specimens with basalt-FRCM.

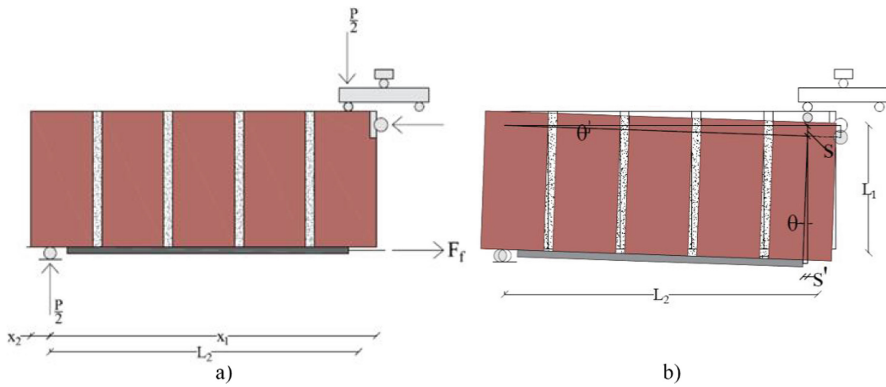


Fig. 5. a) Undeformed shape of the block, b) deformed shape of the block during loading.

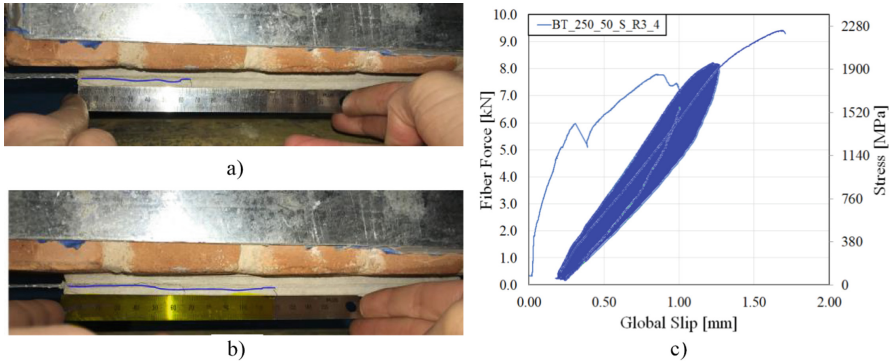


Fig. 6. a) Interfacial crack propagation reading after the first loading-unloading cycle; b) interfacial crack propagation reading after the second loading unloading cycle; c) area between the first and the second cycles.

addition, specimen DT_270_50_S_R1_5 was not considered since it exhibited a load response that was significantly different than others in the same series that failed due to interlaminar failure (MF) (see Fig. 2a).

Regarding specimens with SRG, the average peak force applied to the fibers and global slip to the fibers of the hinged beam tests were larger than those of the single-lap direct shear tests. The average peak force applied to the fibers was 13% larger in the hinge beam test (9.04 kN) than the single-lap test (8.00 kN). The average global slip was 3% larger in the beam test (1.26 mm) than the single-lap shear test (1.23 mm). These results suggest a beneficial effect of the friction generated between the fiber and the matrix in the beam test.

Regarding specimens with basalt-FRCM, the average peak force applied to the fibers and global slip of the hinged beam tests were lower than those of the single-lap direct shear tests. The average peak force applied to the fibers was 8% lower in the beam test (1.33 kN) than the single-lap test (1.45 kN). The average global slip was 53% lower in the beam test (0.62 mm) than the single-lap shear test (1.32 mm). The lower values achieved by the beam tests could be due to the angle created between the fibers and matrix at the beginning of the bonded area due the applied load (see Fig. 4b), which may have caused the fibers to rupture at load levels slightly lower than those of the direct-shear tests. (It should be noted that the basalt fibers were much finer and more brittle than the SRG cords.) Other possible reasons for the discrepancies could be the assumption of perfect symmetry, which may be exacerbated in this study since the specimens had a small number of fiber bundles (3).

Although the hinged beam test is representative of a structural hinge opening in an arch, the discussion above suggests that the results obtained by this test may be influenced by the beneficial or detrimental effects of friction. Another challenge with the beam test is that the values of applied load and global slip in the composite needed to be calculated from measured values of load and displacement of the beam, whereas these values were measured directly in the single-lap direct shear test. For these reasons, the single-lap direct-shear test may be preferred for testing SRG- and basalt FRCM-masonry joints.

4.4 Fracture Energy

Two cycles of loading-unloading were performed on one hinged beam specimen with SRG (namely specimen BT_250_50_S_R1_4) to estimate the matrix-fiber interface fracture energy G_F . At the end of each cycle, the length Δl_i of the interfacial crack (observed from the side of the specimen) was measured (see Fig. 6a and b). The area between the first and the second cycle (see Fig. 6c) represents the energy W^F consumed to extend the interfacial crack by an amount equal to the difference between Δl_2 and Δl_1 . Using the concept of work of fracture, the fracture energy G_F can be determined as:

$$G_F = \frac{W^F}{b_f(\Delta l_2 - \Delta l_1)} \quad (3)$$

The value of W^F (solid area in Fig. 6c) was determined to be 2.006 kN-mm, while the values of Δl_1 and Δl_2 were approximately 65 mm and 119 mm, respectively (Fig. 6a and b). Thus, the resulting fracture energy is $G_F = 740.74$ N/m. This value is consistent with the average value reported by Santandrea et al. [12] for the same composite.

5 Conclusions

In this study, two types of tests, namely the single-lap direct shear test and the hinged beam test, were carried out on SRG and basalt FRCM-masonry joints in order to evaluate and compare the bond capacity of the composite-masonry interface in different load scenarios. The effect of the beam test set-up on the load-carrying capacity of the matrix-fiber interface was investigated. The estimate of the matrix-fiber interfacial fracture energy of SRG-masonry joints was determined through an energy balance approach. Based on the results of this study, the following conclusions can be made:

- The failure mode of specimens with the same fiber type was the same, regardless the test type. In particular, interlaminar failure at matrix-fiber interface was generally observed for SRG-masonry joints, and fiber rupture was observed for basalt FRCM-masonry joints.
- For SRG-masonry joints with the same failure mode and applied load-global slip behavior, the average peak load (average peak stress) in the beam tests was 13% larger than that of the single-lap direct shear tests. The corresponding average global slip at peak load was 3% larger than that of the single-lap direct shear test. These results suggest a beneficial effect of the friction generated between the fiber and the matrix in the beam test.
- For basalt FRCM-masonry joints, the average peak load from the beams test was 8% lower than that of the single-lap direct shear test. Moreover, the average value of the global slip at the peak load registered in the beam test was 53% lower than that of the single-lap direct shear test. This enhanced the non-beneficial effect of the angle created between the matrix and fibers during the beam test, which could lead to breakage of the fiber bundles.

- The fracture energy of the SRG-masonry joint found by measuring two different crack lengths at two different loading-unloading cycles of the hinged beam test was consistent with values reported in the literature.

References

1. Foraboschi P (2004) Strengthening of masonry arches with fiber-reinforced polymer strips 8(3):191–202
2. Valluzzi MR, Valdemarca M, Modena C (2001) Behavior of brick masonry vaults strengthened by FRP laminates. *J Compos Constr* 5(1):163–169
3. Alecci V, De Stefano M, Luciano R, Rovero L, Stipo G (2016) Experimental investigation on bond behavior of cement-matrix-based composites for strengthening of masonry structures *J Compos Constr* 20(1): 04015041
4. Alecci V, Focacci F, Rovero L, Stipo G, De Stefano M (2016) Extrados strengthening of brick masonry arches with PBO – FRCM composites: experimental and analytical investigations. *Compos Struct* 149:184–196
5. Castori G, Borri A, Corradi M (2016) Behavior of thin masonry arches repaired using composite materials. *Compos Part B Eng* 87:311–321
6. Incerti A, Santandrea M, Carloni C, Mazzotti C (2017) Destructive in situ tests on masonry arches strengthened with FRCM composite materials. *Key Eng Mater* 747:567–573
7. Carloni C, Subramaniam KV (2012) FRP-Masonry debonding: numerical and experimental study of the role of mortar joints. *J Compos Constr* 16(5):581–589
8. Ceroni F, Leone M, Rizzo V, Bellini A, Mazzotti C (2017) Influence of mortar joints on the behaviour of FRP materials bonded to different masonry substrates. *Eng Struct* 153:550–568
9. Borri A, Casadei P, Castori G, Hammond J (2009) Strengthening of brick masonry arches with externally bonded steel reinforced composites. *J. Comp. Constr.* 13(6):468–475
10. Santandrea M, Imohamed I, Carloni C, Mazzotti C, Miranda S, Ubertini F (2016) A study of the debonding mechanism in steel and basalt FRCM-masonry joints. In: *Proceedings of the 16th International Brick and Block Masonry Conference*, Padova, Italy, pp 433–440
11. Santandrea M, Daissè G, Mazzotti C, Carloni C (2017) “An investigation of the debonding mechanism between FRCM composites and a masonry substrate. *Key Eng Mater* 747:382–389
12. Santandrea M, Focacci F, Mazzotti C, Ubertini F, Carloni C (2020) Determination of the interfacial cohesive material law for SRG composites bonded to a masonry substrate. *Eng Failure Anal* 111:104322
13. De Stefano M, Luciano R, Focacci F, Stipo G, Alecci V, Rovero L (2017) Strengthening masonry arches with lime-based mortar composite. *Buildings* 7(4):49
14. Calabrese AS, Colombi P, D’Antino T (2019) A bending test set-up for the investigation of the bond properties of FRCM strengthenings applied to masonry substrates. In *Key Eng Mater* 817:149–157
15. Calabrese AS, Colombi P, D’Antino T (2019b) Analytical solution of the bond behavior of FRCM composites using a rigid-softening cohesive material law. *Comp Part B Eng* 174:107051
16. ACI. (2020) Design and construction of externally bonded fabric-reinforced cementitious matrix (FRCM) systems for repair and strengthening concrete and masonry Structures. ACI 549.6R-20. Farmington Hills, MI
17. UNI EN (Italian National Unification Agency). (2011) Methods of test for masonry units. Part 1: Determination of compressive strength. UNI EN 772–1. Milan, Italy: UNI EN

18. EN, B. (2015). 459–1. Building Lime—Part 1: Definitions, Specifications and Conformity Criteria. Brussels, Belgium: BSI, 557, 52
19. ASTM. (2016) Standard test method for compressive strength of hydraulic cement mortars (using 2-in. or [50-mm] cube specimens). ASTM C109/ C109M. West Conshohocken, PA
20. UNI, E. (2004) 998–2 (2004). Specification for mortar for masonry-Masonry mortar 1(2):3
21. Kerakoll Spa, web site: www.kerakoll.com. ASTM. (2011) Standard test method for splitting tensile strength of cylindrical concrete specimens ASTM C496. West Conshohocken, PA
22. ASTM: Standard test method for splitting tensile strength of cylindrical concrete specimens. ASTM C496. West Conshohocken, PA (2011)